Faulty Phase Identification for Transmission Line with Metal Oxide Varistor-protected Series Compensator

Mohammed Hussien Hassan Musa, Ling Fu, Zhengyou He, and Yumin Lei

***Abstract*—The nonlinear operation of metal oxide varistor (MOV)-protected series compensator in transmission lines introduces complications into fault detection approaches. The accuracy of a conventional fault detection schemes is adversely affected by continuous change of the system impedance and load current at the point of a series compensation unit. Thus, this study suggests a method for detecting the faulted phase in MOV-protected series-compensated transmission lines. Primarily, the fault feature is identified using the covariance coefficients of the current samples during the fault period and the current samples during the pre-fault period. Furthermore, a convenience fault detection index is established by applying the cumulative sum technique. Extensive validation through different fault circumstances is accomplished, including different fault positions, resistances, and inception times. The experimental results show that the proposed method performs well with high resistance or impedance faults, faults in noisy conditions, and close-in and far-end faults. The proposed method is simple and efficient for faulty phase detection in MOV-protected series-compensated transmission lines.**

***Index Terms*—Cumulative approach, covariance coefficient, high-impedance fault, response time.**

I. Introduction

THE presence of series compensator devices in power transmission changes the system parameters such as line impedance and load current at the connection point of the series compensation [1]. This is because the series compensator is equipped with a metal oxide varistor (MOV) or a spark-gap for overvoltage protection [2]. Further, the series compensator is invariably part of the fault circuit during the compensation process. This continuous change in the system impedance increases the complexity of relay-setting in conventional distance protection [3]-[5].

An effective method for fault identification in series-compensated transmission lines has been proposed. A previous scheme in [6] has provided techniques for performing fault detection and classification based on the post-fault superimposed energy. However, this scheme is not reliable during a high-impedance fault. Other schemes in [7] and [8] use the super-imposed components to define the fault condition. However, they require a high sampling rate to extract the transient condition, and their fault detection criterion depends on the fault inception angle. The wavelet method combined with the neuro-fuzzy-based method is proposed in [9] for fault diagnosis in a series-compensated transmission line. However, selecting an appropriate wavelet filter is a significant challenge and these filters are insufficient for high impedance faults. A comprehensive intelligent relaying scheme is suggested in [10]. This is dependent on the phase angle of differential impedance, which is obtained based on the ratio of the voltage phasors to the current phasors. Then, the output is input into the data mining model. The proposed data mining model utilizes specified sets of data to train the decision-making algorithm. A scheme in [11] is proposed for identifying fault conditions in series-compensated lines based on a discrete wavelet transform and *k*-nearest neighbor (kNN) algorithm. Machine learning has been utilized to identify fault conditions in [12]. This scheme is accurate up to 96%, but it requires a large neuron in the hidden layer. Chebyshev neural network (ChNN) is employed for carrying out the faults in a series-compensated power line in [13]. ChNN and an undecimated wavelet transform are used in [14] for identification of the fault's zone. In contrast, other schemes [13], [14] utilize specific datasets for training a decision-making algorithm. A pilot protection scheme is proposed in [15] to recognize fault conditions in a series-compensated line. This scheme uses the synchronized samples of two terminals to assess the fault cases in power transmission lines. However, the economic feasibility and complexity of these technologies must be considered when designing and selecting such schemes. The schemes in [16] and [17] provide an adaptive setting for conventional distance relays considering the effects of impedance variation due to MOV operation. However, these schemes still need the pre-definition of the fault section. Cumulative schemes have been proposed for fault detection in [18], [19]. These schemes use the superimposed quantity of the system current and then extract the positive and negative half-cycles individually, which increases the computation burden. A linear regression-based method

Manuscript received: May 11, 2019; accepted: March 6, 2020. Date of Cross-Check: March 5, 2020. Date of online publication: September 1, 2020.

This work was supported by National Natural Science Foundation of China (No. 51777173).

M. H. H. Musa (corresponding author), L. Fu, Z. He, and Y. Lei are with the Electrical Engineering Department, Southwest Jiaotong University, Chengdu, China, and M. H. H. Musa is also with the Electrical Engineering Department, College of Engineering, Almughtarbeen University, Khartoum, Sudan (e-mail: Seadamhd29@yahoo. com; 36196039@qq. com; hezy@swjtu. edu. cn; 449825213@qq.com).

DOI: 10.35833/MPCE.2019.000320

is proposed for fault detection and classification in [20]. This scheme extracts fault features by exploiting the slopes between each adjacent sample during a fault period and then applying cumulative sum (CUSUM) techniques for amplification of the fault feature. The corresponding scheme has failed to detect faults in the case of a MOV-protected series-compensated transmission line. The correlation coefficient-based algorithm is proposed for fault detection and classification in power transmission systems in [21]. This scheme uses the correlation of the current samples during the fault period and the corresponding samples during the pre-fault period to assess the fault condition. However, this scheme shows limitations when identifying faults in MOV-protected series-compensated transmission line.

Given these challenges, a new method is developed for identifying the faulty phases in MOV-protected series-compensated transmission lines. The proposed method compares the covariance indices *CvI* of samples during the fault period with the same samples during the pre-fault period over several cycles and then establishes a convenience fault detection index *FDI* by applying the cumulative-sum (CUSUM) techniques. The main contribution of the new method is its ability to detect high-resistance faults and high-impedance faults in MOV-protected lines. Thus, it is considered a development compared to current schemes [18]-[21] in term of high resistance or impedance faults in MOV-protected series-compensated compensated lines. The conventional CUSUM uses additional computation as it divides the current samples into positive and negative half-cycles. Linear regression coefficient index (*LRCI*) shows limitations with regard to high resistance or impedance faults. Since the fault detection index *LRCI* is obtained using the arithmetic mean of the linear regression coefficient (*LRC*) samples, which decreases the amplitude of *LRCI* during the fault interval, this process adversely affects the performance of the *LRCI* during a high resistance or impedance fault. The correlation coefficient and covariance measure utilize the same concept, unless the correlation coefficient is between −1 and +1. This narrow range adversely affects the performance of the algorithm during the high-resistance faults.

The rest of this paper is defined as follows. The principles of the proposed algorithm is defined in Section II. The simulation and test results are provided in Section III, and the work will be summarized in Section IV.

II. Principles of Proposed Algorithm

The basic intention of the covariance coefficient is to quantify the relationship between two random variables x and y. Therefore, given samples of N datasets of variables, the covariance can be obtained as:

$$Cov = \frac{\sum_{i=1}^{n}(x_i - \bar{x})(y_i - \bar{y})}{N-1} \tag{1}$$

where $\bar{x}$ is the arithmetic mean of x_i; and $\bar{y}$ is the arithmetic mean of y_i. x is taken to be the phase-current samples during the fault period, while y indicates the phase-current samples during the pre-fault interval of the cycle. Therefore, the CUSUM of the covariance samples per cycle is calculated as:

$$CvI(s) = \left| \sum_{j=s-m+1}^{s} Cov(j) \right| \tag{2}$$

where m is the samples per cycle; j is the instantaneous sample; and s is the sampling instant.

Under a safe operation condition, the covariance index stabilizes around a specific value and then changes significantly after the fault inception. This change depends on the relationship between the variables x and y. In general, the covariance index is used for representing how one variable is related to another. Therefore, the covariance is positive when both variables are increasing in the same manner, and negative when the variables are in an opposite relationship. In a power system network, the current is typically prone to changes in direction. Therefore, the covariance index *CvI* may be positive or negative according to the power flow direction. In this paper, it is observed that when a fault happens during the power flow direction from the sending-end bus to the receiving-end bus, *CvI* increases significantly after the fault inception. In contrast, when a fault happens during the power flow direction from the receiving-end to the sending-end, *CvI* decreases significantly after the fault inception. This feature is used for quantifying a convenience *FDI* based on the following expressions:

$$FDI_{F_k} = \max(FDI_{F_k} + CvI_{k-1} - \beta \cdot CvI_0, 0) \tag{3}$$

$$FDI_{R_k} = \min(FDI_{R_k} + CvI_{k-1} - \lambda \cdot CvI_0, 0) \tag{4}$$

where FDI_F is the fault detection index in the case of forward power flow (from sending to receiving end); FDI_R is the fault detection index during reverse power flow; CvI_0 is the reference covariance index as captured in a healthy state; β and λ are the drifting factors chosen to be 2 and 0.75, respectively; and the subscript k is the instantaneous sample of the fault detection index, $k = 1, 2, \ldots, s$. Under a safe operation condition, the output of (3) and (4) are zero. If there is a fault and *CvI* is positive, FDI_F increases abruptly after the fault inception. Simultaneously, the output of (4) will continue to be zero. If there is a fault and *CvI* is negative, FDI_R decreases abruptly after the fault inception. Meanwhile, the output of (3) will continue to be zero. Consequently, a fault condition will be issued if the following criterion is fulfilled:

$$Output = \begin{cases} 1 & FDI_F > 0 \text{ or } FDI_R < 0 \\ 0 & \text{otherwise} \end{cases} \tag{5}$$

where *Output* is the output of (3) and (4).

III. Simulations and Test Results

A power system model built in PSCAD/EMTDC is used for executing the fault tests. The model comprises two power sources (500 kV and 50 Hz) connected through 200 km series-compensated overhead transmission lines. The positive- and negative-sequence impedance of the transmission line is $ZL_1 = ZL_2 = (0.0357 + 0.5078\text{i})\Omega/\text{km}$, and the zero-sequence impedance is $ZL_0 = (0.3632 + 1.3265\text{i})\Omega/\text{km}$. The MOV-protected series compensator includes two stages, and each stage includes series capacitance 193.9 μF with shunt inductance 820.5 μH and resistance 0.0402 Ω. These components are connected shunt with 83.95 kV arrester. The sam-

pling rate is 4 kHz and the data is transferred to MATLAB to implement the fault detection process. Figure 1 shows the schematic diagram of the transmission line, where CB1 and CB2 are circuit breakers.

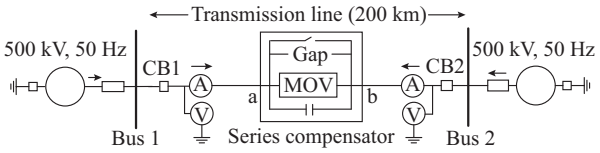

Fig. 1. Schematic diagram of transmission line.

A. Performance of Proposed Method

1) Fault Assessment

Phase-to-ground fault (phase a is ground to earth) at 50 km from Bus 1 with a fault resistance of 200 Ω is selected to validate the performance of the proposed method. The fault inception is at $t = 1.3$ s and it continues for 100 ms. Figure 2(a) illustrates the current waveforms of phase a during the fault and pre-fault periods. Figure 2(b) shows the trajectories of the covariance between current samples during the fault and current samples during the pre-fault period. It can be observed that the trajectory of *CvI* during the pre-fault period stabilizes at a specified limit and then changes significantly after the fault begins. Figure 2(c) illustrates the *FDI* trajectory obtained based on (3). It can be observed that *FDI* is zero until the fault inception and then increases at $t = 1.304$ s. In this case, the fault would have been detected within 4 ms after the fault inception. However, if we consider the time it takes for the CB to begin operating (3 cycles, i.e., about 60 ms) and add a safety margin (approximately 2 cycles), the trip logic would be as in Figure 3. Then, the fault condition shown in Fig. 2 will be cleared within 104 ms of the fault inception.

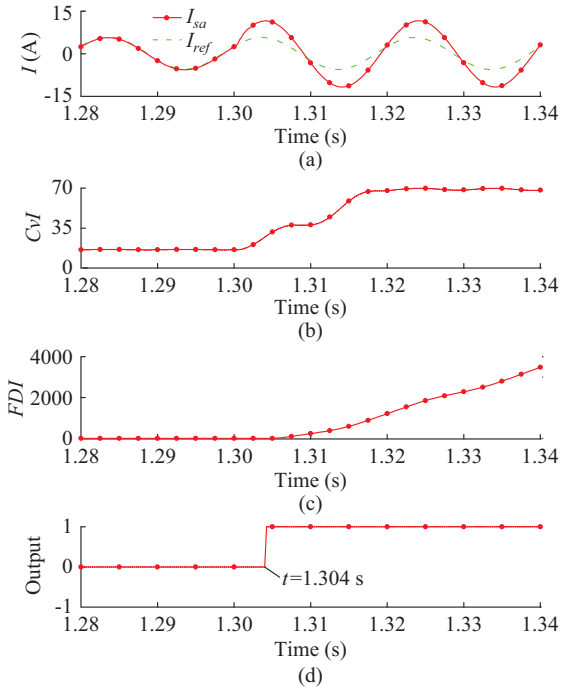

Fig. 2. Performance of proposed method during phase-to-ground fault. (a) Current. (b) *CvI*. (c) *FDI*. (d) Output.

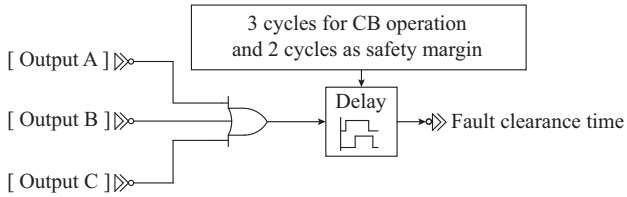

Fig. 3. Logic of fault clearance.

To further evaluate the performance of the proposed scheme, we considered phase-to-ground fault with ground resistance of 15 Ω, which is created at 182 km from Bus 1 (out of the coverage of zone 1). The selected fault starts at $t = 1.1$ s and continues until $t = 1.2$ s. This test is performed with an uncompensated line in case 1, and with a compensated line in case 2, respectively. Figure 4(a) and (b) shows the impedance trajectory recorded by the distance relay located at the sending-end and the trip output, respectively.

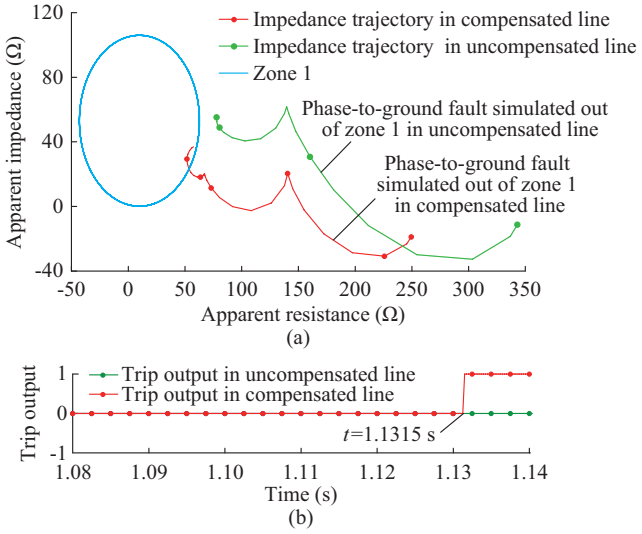

Fig. 4. Performance of distance protection for uncompensated and compensated lines. (a) Impedance trajectory in Mho distance relay. (b) Performance of Mho distance relay during fault cases.

The fault in case 1 is simulated out of zone 1. The impedance trajectory is outside of zone 1 and is not registered by the distance protection. The fault in case 2 is simulated out of zone 1 with MOV-protected series-compensated transmission line, but the impedance trajectory is observed inside zone 1 due to the presence of the MOV-protected series compensator (overreach operation). As the result, the distance protection issues a trip output at $t = 1.1315$ s (about 31.5 ms after the fault inception) as shown in Fig. 4(b). This mal-operation is overcome by the application of the proposed method. Figure 5 shows the performance of the proposed scheme under these conditions, where Fig. 5(a) shows the covariance trajectory for uncompensated and compensated lines, and Fig. 5(b) shows the output trajectories during the corresponding fault. By applying the fault clearance logic, the fault in case 1 would be cleared within 105 ms and that in case 2 would be cleared within 107 ms from the fault registration. In both cases, the proposed scheme has successfully detected the fault faster than the conventional distance protection.

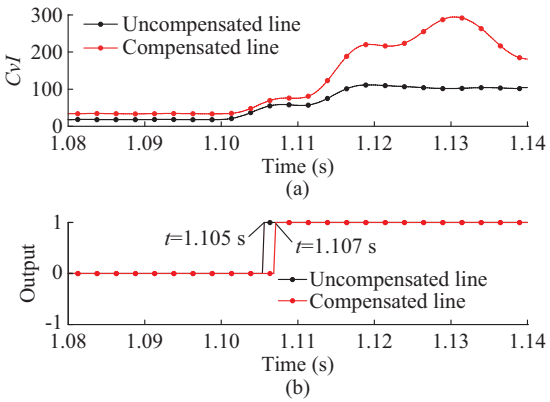

Fig. 5. Performance of proposed method for uncompensated and compensated lines. (a) *CvI*. (b) Output.

To verify the performance of the proposed scheme during double phase fault with series compensation, we considered a double-phase-to-ground fault, i. e., phases a and b are grounded to the earth with ground fault resistance of 100 Ω created at 110 km from bus 1. The selected fault starts at $t=$ 1.3 s and continued until $t=1.4$ s. Figure 6 show the current waveform, *FDI*, and the output trajectories. It can be seen that the *FDI* trajectories of phases a and b jump to the highest value due to a sudden rise in the current signals. Accordingly, the output records a signal after the fault inception at $t=1.305$ s. If the fault clearance logic is applied, the fault would be cleared within 105 ms after the fault is recorded.

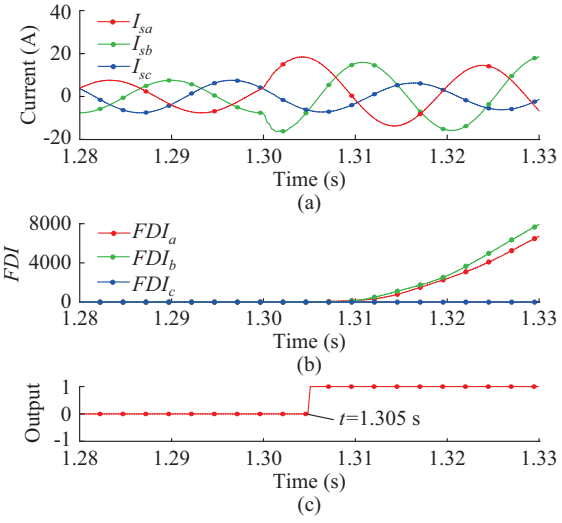

Fig. 6. Proposed method performance during double line fault under series compensation. (a) Current. (b) *FDI*. (c) Output.

Different fault scenarios have been designed to thoroughly investigate the capabilities of the proposed method. The first fault scenario is performed by creating a fault by grounding phase b and phase c at 110 km from the sending-end with different ground fault resistances. The fault cases start at $t=$ 1.25 s and continue until $t=1.3$ s. Table I presents the *FDI* values of the faults. The second fault scenario is accomplished by applying a double-phase fault, i. e., phase a has connected to phase b at 160 km from the sending-end. The fault case is simulated through different time inceptions. Table II presents the *FDI* values for the fault case of phase a connected to phase b. The results in the tables confirm the ability of the proposed method to detect the faulty phase regardless of the fault resistance or fault inception time.

TABLE I
PERFORMANCE WITH DIFFERENT FAULT RESISTANCES

Resistance (Ω)	FDI_a	FDI_b	FDI_c
10	0	62372.0000	60368.0000
100	0	9392.0000	12102.0000
500	0	81.6176	306.5295

TABLE II
PERFORMANCE WITH DIFFERENT INCEPTION TIME INSTANTS

Inception time (s)	FDI_a	FDI_b	FDI_c
1.403	44970	29848	0
1.406	46244	32911	0
1.408	50022	35339	0

2) Close-in Fault Assessment

Close-in faults and direct current (DC) offsets are common causes of current transformer (CT) saturation. The highest DC offset occurs when a fault begins at a fault inception angle (FIA) of −90° or +90°. To evaluate the performance of the proposed method under such conditions, the proposed method is tested by creating a close-in fault with an FIA of 90°. The CT set is selected with a 5 Ω burden and a turn ratio of 1000∶5 installed at the sending-end. A three-phase-to-ground fault situated at $FIA\approx 90°$ ($t=1.443$ s), which is 10 km from bus 1, is considered to execute the CT saturation test. The fault case is performed with ground fault resistance ($R_f\approx 10$ Ω). Figure 7 shows the current waveforms and the *CvI* and *FDI* trajectories during the corresponding fault.

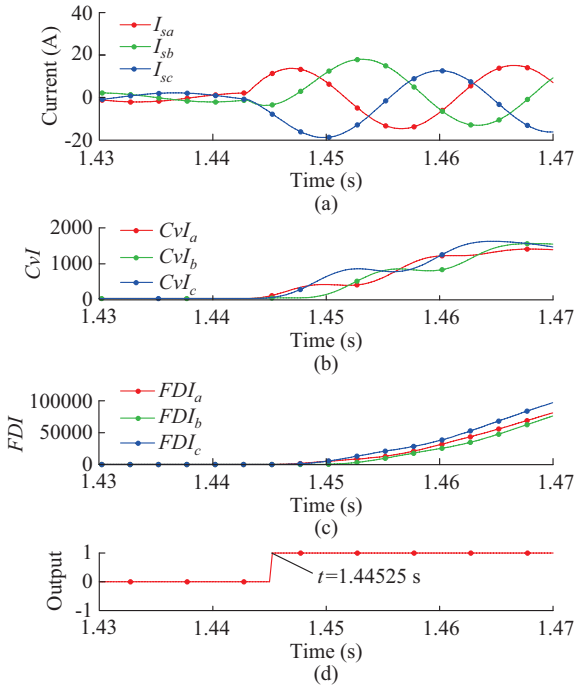

Fig. 7. Performance of proposed method under close-in fault. (a) Current. (b) *CvI*. (c) *FDI*. (d) Output.

The fault case is detected correctly with remarkable timing. It is cleared 102.25 ms after the fault begins. This test is repeated several times with different CT burdens. Table III shows the corresponding *FDI* and the time required for each fault detection. The results confirm that the proposed method is not influenced by a change in CT burden.

TABLE III
PERFORMANCE IN DIFFERENT OPERATION MODES

Burden (Ω)	FDI_a	FDI_b	FDI_c	Time (ms)
5	152080	146210	166190	102.25
10	152080	146210	166190	102.25
20	152070	143950	159010	102.25

3) Noise Test

A noise test is executed by applying double-phase-to-ground fault, i.e., phases a and c are grounded to earth with a ground resistance R_f of 100 Ω. The fault case is carried out 110 km from bus 1. It starts at $t = 1.15$ s and continues until $t = 1.25$ s. Phase a is corrupted with noise of 20 dB, while phases b and c remain clear of noise. Figure 8(a) shows the current waveforms, while Fig. 8(b)-(d) shows the *CvI*, *FDI*, and the output trajectories, respectively. It is possible to conclude that the noise has no effect on the performance of the proposed method. Furthermore, the fault case could be cleared within 108.75 ms including the fault clearance logic. These results demonstrate the exceptionality of the performance of the proposed method in situations with noise.

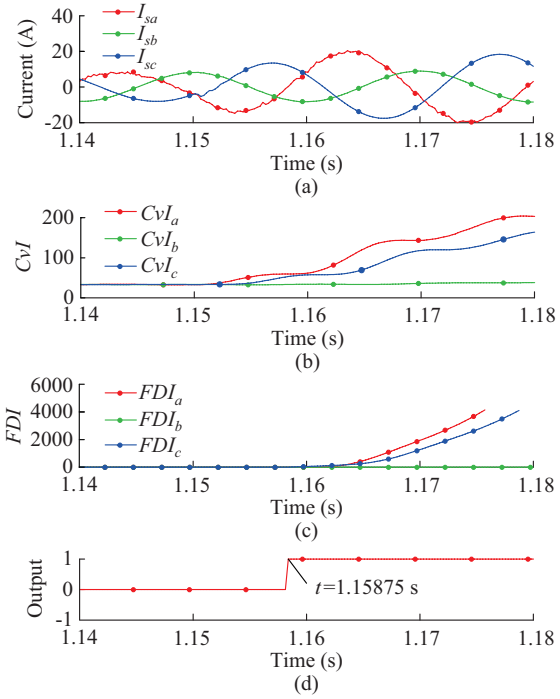

Fig. 8. Performance of proposed method under noise condition. (a) Current. (b) *CvI*. (c) *FDI*. (d) Output.

4) Change of Power Flow Direction

The change of power flow direction is caused by the reversal of the power angle of the voltage source. However, such conditions will also change the covariance from a positive relationship to a negative relationship. This test is executed by changing the sending voltage source angle δ_1 from 30° (default) to 10°, and the receiving voltage source angle δ_2 from 10° (default) to 30°. Then, phase-to-ground fault has been applied, where phase b is grounded to earth with a ground resistance of 100 Ω, and the fault case is 10 km away from the series compensation unit. The fault case starts at $t = 1.5$ s and continues until $t = 1.6$ s. Figure 9(a) - (c) shows the *CvI* trajectory, *FDI* trajectory, and the output, respectively, when a power flow has changed its direction. The figure shows that the covariance trajectory decreases significantly after the fault inception. This is caused by the covariance reversed in its relation-direction from positive to negative covariance due to the reverse of power flow. Therefore, the fault case is cleared satisfactorily within 108 ms after the fault inception. It is evident that the proposed scheme is not adversely affected by the change in power flow direction.

Table IV contains the *FDI* values in the case of phases a and b grounded to earth, which is simulated 10 km away from the sending-end with different power flow directions. It is observed that the positive indices indicate the faulty phase, and that in the second case, the negative indices indicate the faulty phases. Therefore, the change of power flow direction does not affect the final evaluation of the proposed method.

TABLE IV
PERFORMANCE DURING POWER FLOW CHANGE

δ_1 (°)	δ_2 (°)	FDI_a	FDI_b	FDI_c
30	5	7549.0	12768.0	0
5	30	–3728.6	–3212.3	0

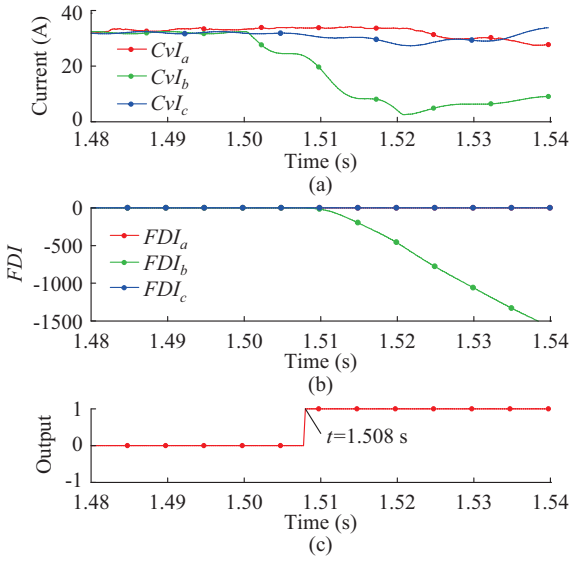

Fig. 9. Performance of proposed method with change of power flow direction. (a) Current. (b) *FDI*. (c) Output.

5) Sampling Frequency

The average number of samples that can be obtained within 1 s is a crucial factor in the assessment of the perfor-

mance of fault detection algorithms. A higher sampling rate allows for a considerable increase in signal resolution. However, it also increases the burden on relays and the microprocessor. The proposed scheme functions properly at different sampling rates ranging from 1 kHz up to 5 kHz. Phases a and b are grounded with a fault resistance of 100 Ω selected to perform this test. The corresponding fault at 110 km from the sending-end, which starts at $t = 1.1$ s and continues for 100 ms. The results are shown in Table V. At higher sampling rates, the response time is reduced. However, there is not a noticeable difference in the response time when the sampling frequency is 4 or 5 kHz. Therefore, 4 kHz is chosen as the sampling frequency for the proposed method.

TABLE V
PERFORMANCE WITH DIFFERENT SAMPLING RATES

Sampling frequency (kHz)	FDI_a	FDI_b	FDI_c	No. of samples per cycle	Response time (ms)
1	21331	28667	0	20	106.00
2	41195	55560	0	40	104.50
4	8187	11089	0	80	103.75
5	10123	13849	0	100	103.60

6) High-impedance Fault Assessment

The high-impedance fault model reported in [22], [23] is utilized to assess the performance of the proposed method. It consists of two amplified diodes D_p and D_n, two DC sources V_p and V_n, and variable resistances R_p and R_n (400 Ω and 600 Ω, respectively), as shown in Fig. 10.

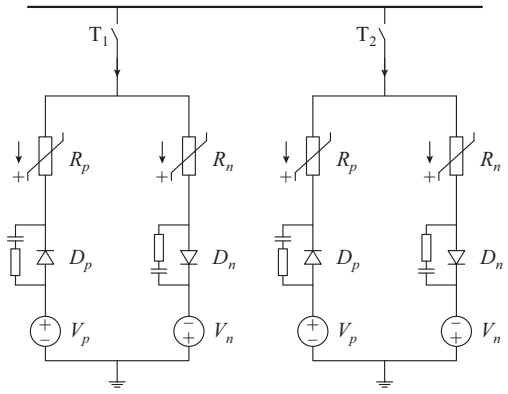

Fig. 10. High-impedance model.

The DC voltage continuously varies around 0.01 ms. Whenever the system voltage is greater than V_p, the current will flow towards the ground. It will reverse when the system voltage is less than V_n. No current will flow when the system voltage is greater than V_n and less than V_p [22]-[24]. To evaluate the performance of the proposed method for a high-impedance fault, a high-impedance fault is implemented at 110 km from the sending end that starts at $t = 1.35$ s and continues for 100 ms after the fault inception.

Figure 11(a)-(c) shows *CvI*, *FDI* and the output trajectories during the corresponding fault, respectively. When applying the fault clearance logic, it is obvious that a fault detected within 15 ms would be cleared within 115 ms after the fault inception.

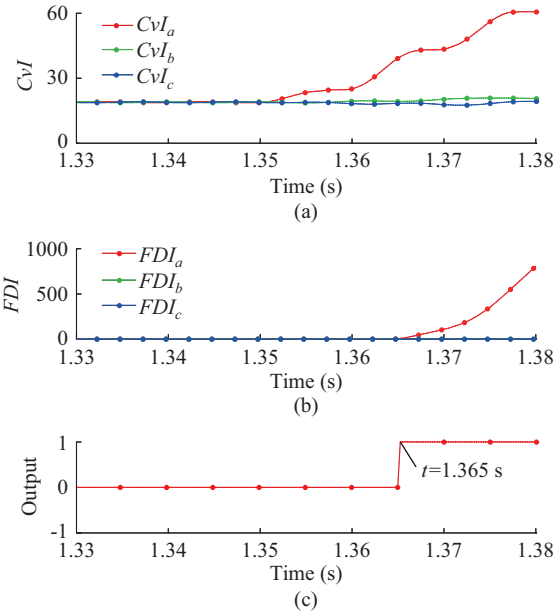

Fig. 11. High-impedance fault assessment. (a) Current. (b) *FDI*. (c) Output.

7) Performance in Multi-machine Systems

The IEEE 9-bus system is considered for further investigation of the proposed method. Figure 12 shows the employed schematic diagram of the IEEE 9-bus system. It has been established in PSCAD/EMTDC by Manitoba HVDC Research Center. In this test, phases a and b are grounded to earth at F1 and F2, respectively. The fault case starts at $t = 1.5$ s and continues until $t = 1.6$ s. The ground fault resistance is set to be 100 Ω. The variables β and λ used in (3) and (4) are set to be 1.25 and 0.8, respectively. SM1, SM2, and SM3 represent synchronous machine 1, 2, and 3, respectively.

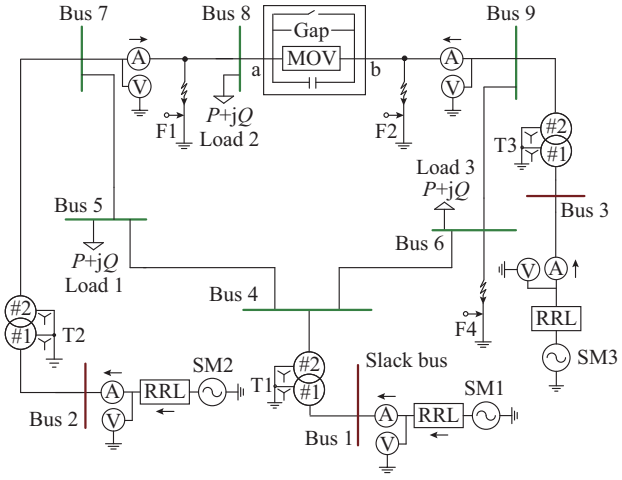

Fig. 12. IEEE 9-bus system.

Figure 13(a) shows *CvI*, *FDI* and the output when the fault occurs at F1, 50 km from the sending-end (group a). Figure 13(b) shows *CvI*, *FDI* and the output when the fault

occurs at F2, 50 km from the compensation unit (group b). It is evident that the proposed method is capable of identifying the faulty phase in a multi-machine system correctly.

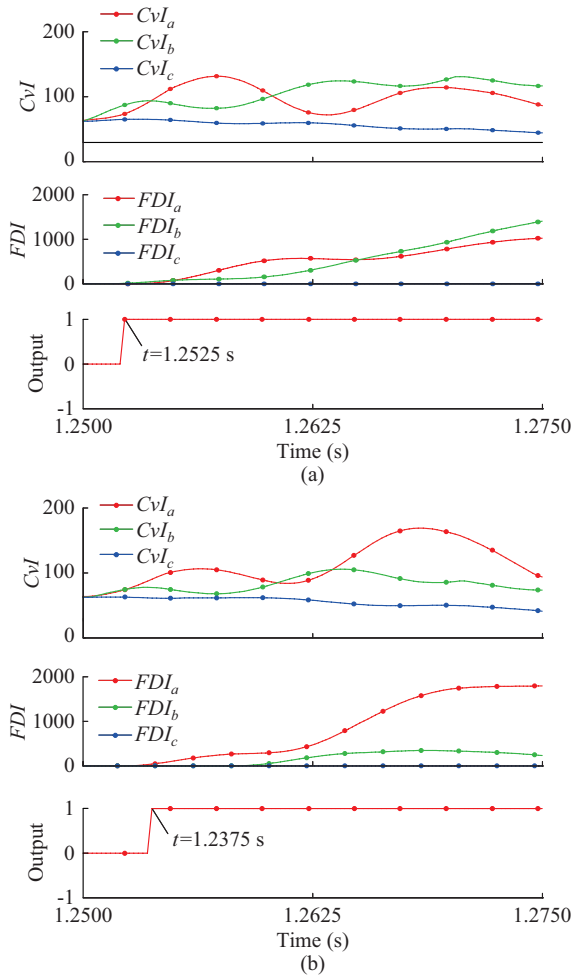

Fig. 13. Performance in multi-machine systems. (a) Group a. (b) Group b.

B. Comparison with Previous Work

Far-end fault with high impedance or resistance in MOV-protected series-compensated transmission lines is a challenge for many fault detection methods. The proposed method has been compared with schemes in [18]-[21] because it uses the same concept of using a covariance measurement in a cumulative manner. The schemes in [18], [19] use a CUSUM-based technique for fault detection in power system relay applications. To evaluate the performance of the proposed method related to these schemes [18], [19], a high-impedance fault is considered in phase a, which is at 160 km from the sending-end. Figure 14(a) shows the current waveform, and Fig. 14(b) and (c) shows the positive and negative fault detector indices and the output of the other schemes [18], [19], respectively. It is obvious that the schemes in Fig. 14(b) [19] fail to detect the fault condition. Meanwhile, the scheme in Fig. 14(c) [18] appears to be unstable. It issues a high trigger at $t = 1.324$ s, which is not correct. On the other hand, the performance of the proposed scheme during the test is shown in Fig. 14(d). Herein, the fault case is detected successfully at $t = 1.3655$ s.

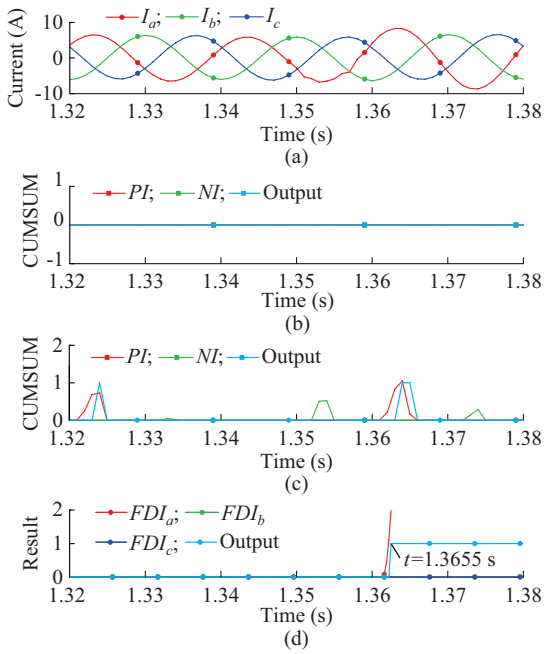

Fig. 14. Proposed scheme compared to two schemes in [18], [19]. (a) Current. (b) Results of CUMSUM. (c) Results of ACUMSUM. (d) Results of proposed method.

Recently, other schemes [20], [21] have been proposed, which offer advantages over traditional methods in terms of fault detection speed. Further, they are immune to noises in the current signals during the fault. However, they are less reliable against high-impedance or resistance faults in MOV-protected series-compensated transmission lines. To verify this situation, a high-impedance fault is set at 160 km from bus 1 in phase a. The fault case starts at $t = 1.35$ s and continues until $t = 1.45$ s. The variable resistances $R_p = 450\ \Omega$, $R_n = 600\ \Omega$. Figure 15 shows the performance of the proposed scheme against the linear regression-based method [20], which uses the difference between the current signal slopes of each sample recorded during the fault period as an indication for a fault condition. Figure 15(a) shows the current waveform and Fig. 15(b) shows the response of the scheme [20] to the fault condition. It is evident that the scheme fails to detect the fault condition.

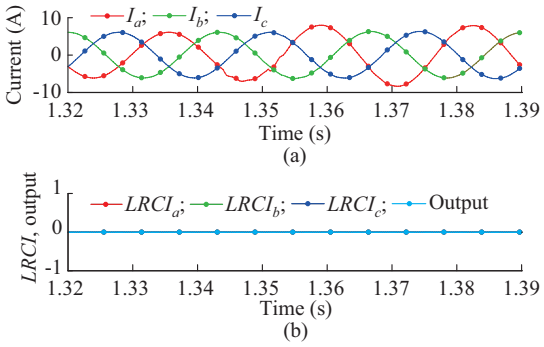

Fig. 15. Performance of proposed method compared to scheme in [20]. (a) Current. (b) *LRCI* and output.

The same fault is repeated for testing the next scheme [21], which uses a method that involves the computation of

the correlation between the current samples during the fault period with the current samples during the pre-fault period in order to determine the fault condition. In this test, the fault condition is detected if the correlation coefficient index (CCI) is less than 0.9. Otherwise, the system is considered to be running in the healthy state. The performance of the proposed method related to the correlation coefficient based algorithm is shown Fig. 16. It is obvious that the CCI trajectory decreases to the lowest value during the fault period but does not exceed the threshold (0.9). Thus, the scheme fails to detect the fault condition. Therefore, this method has low effectivity during a high-resistance or impedance fault. For further comparison of the performance of the proposed scheme with those of other schemes [20], [21], different types of faults including single-phase, double-phase, and three-phase are considered. The selected faults are created at 160 km from the sending-end and the test is performed with different ground resistances. Table VI provides the *FDI* for the comparative schemes and the proposed method. The results confirm that the comparative schemes are adversely affected by the additional impedance due to the presence of a series compensator in the fault path. The proposed method is superior in terms of high impedance or resistance in MOV-protected series-compensated transmission lines.

Generally, it is possible to conclude that the proposed method is characterized by the following remarks.

1) The proposed scheme avoids dividing the current signals into positive and negative half-cycles used in two other schemes [18], [19], which reduces the computation burden.

2) The proposed method detects the fault condition based on obtaining the relationship between the current samples during fault intervals and pre-fault intervals, but it is not restricted to a narrow range as in another scheme [21].

3) The proposed scheme works properly with high-resistance or impedance faults compared with the scheme in [20], because the latter uses the mean value for LRC to dampen the ripple in the LRC output, which reduces the reliability of LRCI scheme against the high-resistance or impedance faults.

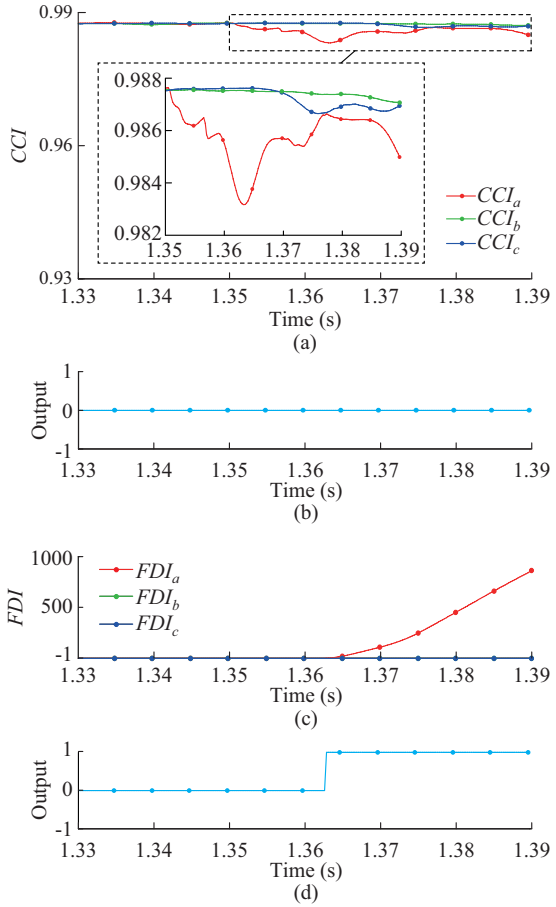

Fig. 16. Performance of proposed method compared with scheme in [21]. (a) *CCI* in group a. (b) Output in group a. (c) *FDI* in group b. (d) Output in group b.

TABLE VI
PERFORMANCE OF SCHEMES FOR DIFFERENT TYPES OF FAULTS AT DIFFERENT LOCATIONS WITH DIFFERENT RESISTANCES

Scheme	Fault resistance (Ω)	Fault type	FDI_a	FDI_b	FDI_c	Response time (ms)	Assessment
[20]	100	Phase-to-ground	0.6901	0	0	105.00	Detected correctly
		Double-phase-to-ground	0.7932	1.6010	0	105.00	Detected correctly
		Three-phase-to-ground	0.7835	0	0.3930	-	Failed
	200	Phase-to-ground	0.2757	0	0	109.50	Detected correctly
		Double-phase-to-ground	0.3080	0	0.1371	-	Failed
		Three-phase-to-ground	0.3095	0	0	-	Failed
[21]	100	Phase-to-ground	0.9712	0.9841	0.9838	-	Failed
		Double-phase-to-ground	0.9722	0.9632	0.9872	-	Failed
		Three-phase-to-ground	0.9701	0.9653	0.9701	-	Failed
	200	Phase-to-ground	0.9829	0.9869	0.9865	-	Failed
		Double-phase-to-ground	0.9822	0.9796	0.9875	-	Failed
		Three-phase-to-ground	0.9816	0.9795	0.9813	-	Failed
Proposed method	100	Phase-to-ground	3867.2000	0	0	103.50	Detected correctly
		Double-phase-to-ground	4084.6000	4270.8000	0	103.50	Detected correctly
		Three-phase-to-ground	4750.7000	4334.3000	2563.1000	103.50	Detected correctly
	200	Phase-to-ground	1429.4000	0	0	107.30	Detected correctly
		Double-phase-to-ground	1511.8000	1521.2000	0	109.25	Detected correctly
		Three-phase-to-ground	1727.0000	1555.6000	196.2000	106.75	Detected correctly

IV. Conclusion

The proposed method is suggested to identify the faulty phase in MOV-protected series-compensated transmission lines. It relies on calculating the covariance between the current samples over several cycles during the fault period and the pre-fault period. Moreover, the covariance index between these current samples are stable around a specific limit under the safe operation condition, and significant changes arise during the fault period. Then, the CUSUM technique is employed to enlarge the fault feature. As a result, the proposed method can be characterized by: ① less computation, which relies only on the current measurement and does not divide the current signals into positive and negative half-cycles as in conventional cumulative schemes; ② good immunity to noise, which works properly with signal-noise ratio (SNR) up to 20 dB; ③ proper performance with far-end, high-resistance or impedance faults in MOV-protected series-compensated transmission lines; ④ proper performance with different sampling rates from 1 kHz up to 5 kHz; ⑤ remarkable time response, which does not exceed 15 ms in the worst test case.

References

[1] A. M. El-Zonkoly and H. Desouki, "Wavelet entropy based algorithm for fault detection and classification in FACTS compensated transmission line," *International Journal of Electrical Power & Energy Systems*, vol. 33, no 8, pp. 1368-1374, Oct. 2011.

[2] M. E. Mandour and A. A. Elalaily, "Swivelling characteristic for the protection of series compensated lines," *Electric Power Systems Research*, vol. 18, no. 1, pp. 31-35, Jan. 1990.

[3] A. Capar and A. B. Arsoy, "A performance oriented impedance based fault location algorithm for series compensated transmission lines," *International Journal of Electrical Power & Energy Systems*, vol. 71, pp. 209-214, Oct. 2015.

[4] R. K. Gajbhiye, B. Gopi, P. Kulkarni *et al.*, "Computationally efficient methodology for analysis of faulted power systems with series-compensated transmission lines: a phase coordinate approach," *IEEE Transactions on Power Delivery*, vol. 23, no. 2, pp. 873-880, Apr. 2008.

[5] B. Vyas, R. P. Maheshwari, and B. Das, "Protection of series compensated transmission line: issues and state of art," *Electric Power Systems Research*, vol. 107, no. 2, pp. 93-108, Feb. 2014.

[6] O. H. Gupta and M. Tripathy, "Superimposed energy-based fault detection and classification scheme for series-compensated line," *Electric Power Components and Systems*, vol. 44, no. 10, pp. 1095-1110, May 2016.

[7] P. Jafarian and M. Sanayepasand, "High-speed superimposed-based protection of series-compensated transmission lines," *IET Generation, Transmission & Distribution*, vol. 5, no 12, pp. 1290-1300, Dec. 2011.

[8] N. Perera and A. D. Rajapakse, "Series-compensated double-circuit transmission-line protection using directions of current transients," *IEEE Transactions on Power Delivery*, vol. 28, no. 3, pp. 1566-1575, Jul. 2013.

[9] H. Eristi, "Fault diagnosis system for series compensated transmission line based on wavelet transform and adaptive neuro-fuzzy inference system," *Measurement*, vol. 46, no. 1, pp. 393-401, Jan. 2013.

[10] M. K. Jena and S. R. Samantaray, "Intelligent relaying scheme for series-compensated double circuit lines using phase angle of differential impedance," *International Journal of Electrical Power & Energy Systems*, vol. 70, pp. 17-26, Sept. 2015.

[11] A. Swetapadma, P. K. Mishra, A. Yadav *et al.*, "A non-unit protection scheme for double circuit series capacitor compensated transmission lines," *Electric Power Systems Research*, vol. 148, pp. 311-325, Jul. 2017.

[12] V. Malathi, N. S. Marimuthu, S. Baskar *et al.*, "Application of extreme learning machine for series compensated transmission line protection," *Engineering Applications of Artificial Intelligence*, vol. 24, no. 5, pp. 880-887, Aug. 2011.

[13] B. Vyas, B. Das, and R. P. Maheshwari, "Improved fault classification in series compensated transmission line: comparative evaluation of Chebyshev neural network training algorithms," *IEEE Transactions on Neural Networks*, vol. 27, no. 8, pp. 1631-1642, Aug. 2016.

[14] B. Vyas, B. Das, and R. P. Maheshwari, "An improved scheme for identifying fault zone in a series compensated transmission line using undecimated wavelet transform and Chebyshev neural network," *International Journal of Electrical Power & Energy Systems*, vol. 63, pp. 760-768, Dec. 2014.

[15] C. Wang, G. Song, X. Kang *et al.*, "Novel transmission-line pilot protection based on frequency-domain model recognition," *IEEE Transactions on Power Delivery*, vol. 30, no. 3, pp. 1243-1250, Jun. 2015.

[16] O. V. Sivov, H. A. Abdelsalam, and E. B. Makram, "Adaptive setting of distance relay for MOV-protected series compensated line considering wind power," *Electric Power Systems Research*, vol. 137, pp. 142-154, Aug. 2016.

[17] M. Biswal, "Adaptive distance relay algorithm for double circuit line with series compensation," *Measurement*, vol. 53, pp. 206-214, Jul. 2014.

[18] M. R. Noori and S. M. Shahrtash, "Combined fault detector and faulted phase selector for transmission lines based on adaptive cumulative sum method," *IEEE Transactions on Power Delivery*, vol. 28, no. 3, pp. 1779-1787, Jul. 2013.

[19] S. R. Mohanty, A. K. Pradhan, and A. Routray, "A cumulative sum-based fault detector for power system relaying application," *IEEE Transactions on Power Delivery*, vol. 23, no. 1, pp. 79-86, Jan. 2008.

[20] M. H. Musa, Z. He, L. Fu *et al.*, "Linear regression index-based method for fault detection and classification in power transmission line," *IEEJ Transactions on Electrical and Electronic Engineering*, vol. 13, no. 9, pp. 979-987, Jul. 2018.

[21] M. H. H. Musa, Z. He, L. Fu *et al.*, "A correlation coefficient-based algorithm for fault detection and classification in a power transmission line," *IEEJ Transactions on Electrical and Electronic Engineering*, vol. 13, no. 7, pp. 1394-1403, Jul. 2018.

[22] I. Hafidz, P. E. Nofi, D. O. Anggriawan *et al.*, "Neuro wavelet algorithm for detecting high impedance faults in extra high voltage transmission systems," in *Proceedings of 2017 2nd International Conference on Sustainable and Renewable Energy Engineering (ICSREE)*, Hiroshima, Japan, May 2017, pp. 97-100.

[23] W. D. C. Tat and Y. Xia, "A novel technique for high impedance fault identification," *IEEE Transactions on Power Delivery*, vol. 13, no. 3, pp. 738-744, Jul. 1998.

[24] A. M. Sharaf and G. Wang, "High impedance fault detection using feature-pattern based relaying," in *Proceedings of IEEE PES Transmission and Distribution Conference and Exposition*, Dallas, USA, Sept. 2003, pp. 222-226.

Mohammed Hussien Hassan Musa received the B.Sc. and M.Sc. degrees in electrical engineering from Sudan University of Science and Technology, Khartoum, Sudan, in 2005 and 2010, and the Ph.D. degree from Southwest Jiaotong University, Chengdu, China, in 2018, respectively. He worked in National Electricity Corporation (NEC), Khartoum, Sudan, from 2006 to 2010. He now works as Assistant Professor in College of Engineering, Almughtarbeen University, Khartoum, Sudan, and as Senior Technical Support at Sudanese Thermal Power Generating Company (STPG), Khartoum, Sudan. His research interests include faults diagnosis of power systems, stability studies, and smart grid integration with the sustainable energies.

Ling Fu received the Ph.D. degree from the Department of Electrical Engineering, Southwest Jiaotong University, Chengdu, China, in 2010. She did her post-doctoral research at the University of Tennessee, Knoxville, USA, in 2011. She is currently with the Department of Electrical Engineering, Southwest Jiaotong University. Her research interests include power system stability and control, signal processing, and wide-area protection.

Zhengyou He received the B.Sc. and M.Sc. degrees from Chongqing University, Chongqing, China, in 1992 and 1995, respectively, and the Ph.D. degree in electrical engineering from Southwest Jiaotong University, Chengdu, China, in 2001. Since 2002, he has been a Professor at the College of Electrical Engineering, Southwest Jiaotong University. His research interests include signal processing and information theory and its application in power systems, and wavelet transforms application in power system.

Yumin Lei received the B.S. degree from the Department of Electrical Engineering, Hubei University of Technology, Wuhan, China, in 2013, and the M.S. degree from the Department of Electrical Engineering, Southwest Jiaotong University, Chengdu, China, in 2020. Currently, he is an Assistant Engineer of electrical engineering at Central and Southern China Municipal Engineering Design & Research Institute Co., Ltd., Wuhan, China. His research interest includes comprehensive automation in power systems.